sciendo

LATVIAN JOURNAL OF PHYSICS
AND TECHNICAL SCIENCES
2024, N 2

DOI: 10.2478/lpts-2024-0008

RED PERSISTENT LUMINESCENCE AND TRAP PROPERTIES OF Mg_2SiO_4: Mn^{2+}, M^{3+} (M^{3+} = B^{3+}; Al^{3+}; Ga^{3+}; In^{3+}) MATERIAL

G. Doke

Institute of Solid State Physics, University of Latvia,
8 Kengaraga Str., Riga, LV-1063, LATVIA
E-mail: guna.doke@cfi.lu.lv

Persistent luminescence (PersL), also called long-lasting phosphorescence or simply afterglow, is a luminescence characterised by the emission of radiation from a few seconds to several days after the excitation source has been switched off. Over the past two decades, research on PersL materials, both in fundamental and applied physics, has developed rapidly; however, the explanation for the physical processes that cause afterglow still needs to be clarified. Today, PersL materials are used mainly for luminescent paints, safety signs and decorations. At the same time, research into using such materials in medicine, information storage, anti-counterfeiting technology, etc., is underway.

Currently, information on the long persistent luminescence materials with emission in the blue and green spectral range is widely available. In contrast, the number of publications on the afterglow in the red and near-infrared spectral range is considerably lower.

Within the framework of this research, Mg_2SiO_4: Mn^{2+}; M^{3+} (M^{3+} = B^{3+}; Al^{3+}; Ga^{3+}; In^{3+}) materials were synthesised using solid state reaction synthesis. When excited with X-rays, the materials exhibited a broad Mn^{2+} PersL band with two maxima at approximately 625 nm and 730 nm. After cessation of irradiation, an afterglow of at least 6 hours could be observed.

The research focuses on the trap properties of the materials. It was concluded that at least three discrete trap levels with activation energies approximately between 0.4–1.6 eV were present in the samples. Additionally, co-doping with Al^{3+}; Ga^{3+}; In^{3+} ions improved PersL longevity of the Mg_2SiO_4: Mn^{2+} material.

Keywords: *Activation energy, Mn^{2+}, persistent luminescence, thermally stimulated luminescence, traps.*

1. INTRODUCTION

Persistent luminescence (PersL) is a type of luminescence that involves the emission of radiation even after the irradiation source has been turned off. This delayed emission occurs due to the trapping of charge carriers by point defects in crystals, which function as trapping sites. The charge carriers are gradually released and then recombine at luminescence centres. However, the mechanism behind PersL is still not fully comprehended [1]–[3].

PersL materials are generally utilised for low-tech purposes like luminescent paints, safety signs, and decorative items. However, there are ongoing research and development efforts to explore their potential in fields like medicine, military technology, and anti-counterfeiting [4]–[6]. While most well-developed PersL materials emit light in the visible part of the spectrum, particularly green, there is relatively less research on materials with emission bands in the red region. The most prominent red light-emitting PersL materials are Y_2O_2S: Eu^{3+}, Mg^{2+}, Ti^{4+} [7], $Ca_{1-x}Sr_xS$: Eu^{2+} [8] and others [9]–[11]. However, using rare-earth ions significantly increases the cost of material production. As an alternative, Mn^{2+} is commonly suggested. As a transition metal, Mn^{2+} is strongly affected by the crystal field surrounding it and, when introduced into a properly chosen matrix, can provide red luminescence.

Mg_2SiO_4 phosphors have garnered considerable scientific interest since the 1990s; however, most publications have focused on photoluminescence instead of PersL. The afterglow properties of Mn^{2+} doped Mg_2SiO_4 have been discussed in the context of optical properties of Mg_2SiO_4: Mn^{2+}, Dy^{3+} [12] and Mn-doped Mg_2SiO_4-Mg_2GeO_4 solid solution [13].

Co-doping is a commonly used method for developing exceptional PersL phosphors, where co-doped ions can function as electron "pumps" for enhanced trapping efficiency [14] or as trapping centres [15]. Commonly an aliovalent substitution is used since if ions with different charges substitute the cations or anions in the host, additional defects will be produced to ensure charge compensation [16]–[18]. Therefore, in this publication, samples of Mg_2SiO_4: 0.1 mol% Mn^{2+}; 0.5 mol% M^{3+} (M^{3+} = B^{3+}; Al^{3+}; Ga^{3+}; In^{3+}) were synthesised, and their PersL and trap properties were analysed.

2. EXPERIMENTAL

2.1. Synthesis

Mg_2SiO_4: 0.1 mol% Mn^{2+}; 0.5 mol% M^{3+} (M^{3+} = B^{3+}; Al^{3+}; Ga^{3+}; In^{3+}) samples were synthesised by a conventional solid-state synthesis method. During the synthesis, stoichiometric amounts of the following chemical compounds: $MgCO_3{\cdot}Mg(OH)_2{\cdot}xH_2O$ (99.996%, Alfa Aesar), where $x \approx 3$, SiO_2 (99.9999%, Alfa Aesar), MnO_2 (99.997%, Alfa Aesar), B_2O_3 (99.999%, Alfa Aesar), Al_2O_3 (99.999%, Alfa Aesar), Ga_2O_3 (99.999%, Alfa Aesar) and In_2O_3 (99.999%, Alfa Aesar) were weighted. The mixture was ground in a marble mortar, transferred into a corundum crucible, and annealed at 1450 °C for 2 h in an ambient atmosphere to obtain polycrystalline Mg_2SiO_4: Mn^{2+}, M^{3+} (M^{3+} =

B^{3+}; Al^{3+}; Ga^{3+}; In^{3+}) samples. A heating and cooling rate of 5 °C/min was applied. For heat treatment, a high-temperature furnace Carbolite HTF18 was used. In this paper, Mg_2SiO_4 materials will be denominated as MSO.

2.2. Characterisation

X-ray diffraction (XRD) patterns were measured by MiniFlex 600 RIGAKU X-ray diffractometer. The International Centre for Diffraction Data card for Mg_2SiO_4 (PDF 01-084-1402) was used as a reference.

PersL spectra, PersL decay profiles, and thermally stimulated luminescence (TSL) curves were measured using a Lexsyg research – Fully Automated TL/OSL Reader from Freiberg Instruments GmbH coupled with photomultiplier Hamamatsu R13456. X-ray tube VF-50 J/S (40 kV, 0.5 mA, W-anode) was used as an irradiation source. The system operated at a linear heating rate in the temperature range between room temperature and 400 °C. Isothermal PersL decay curves were recorded at 25 °C.

3. RESULTS AND DISCUSSION

3.1. Structure Analysis

The structure of MSO samples was characterised by XRD measurements. The obtained XRD patterns and standard cards PDF 01-084-1402 corresponding to orthorhombic Mg_2SiO_4 are shown in Fig. 1. The peak positions of the samples matched well with the PDF patterns, and no additional phases could be identified, confirming the formation of single phase Mg_2SiO_4 material and complete incorporation of dopants into host matrix.

The crystal structure of the Mg_2SiO_4 compound is shown in Fig. 2. There are three types of polyhedrons present in the structure: [SiO_4] tetrahedron and two slightly dissimilar [MgO_6] octahedrons, one of which is more distorted. The two different cation octahedra form alternating chains parallel to the c-axis [19].

The ionic radii of the present cations at four-fold and six-fold coordination are given in Table 1. According to the ionic radii and the valence, Mn^{2+} ions most likely occupy both Mg^{2+} sites. As for co-dopants, B^{3+}, Al^{3+}, Ga^{3+}, and In^{3+}, it is difficult to draw a firm conclusion since not only radii difference has to be considered but also varied valence. Nevertheless, it can be speculated that Ga^{3+} and In^{3+} ions substitute Mg^{2+}, while the positions of B^{3+} and Al^{3+} cannot be clearly determined.

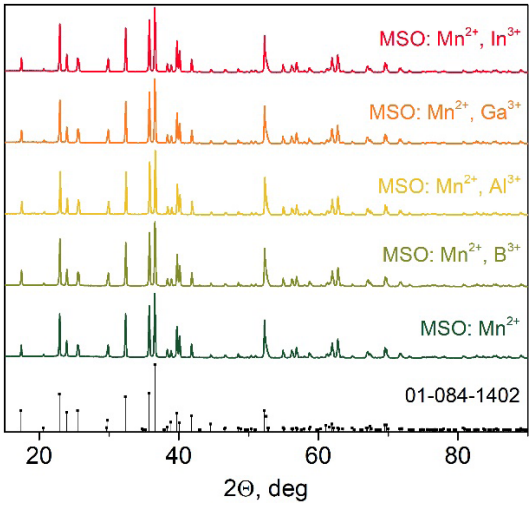

Fig. 1. XRD patterns of MSO samples and theoretical position of Mg_2SiO_4 (PDF 01-084-1402).

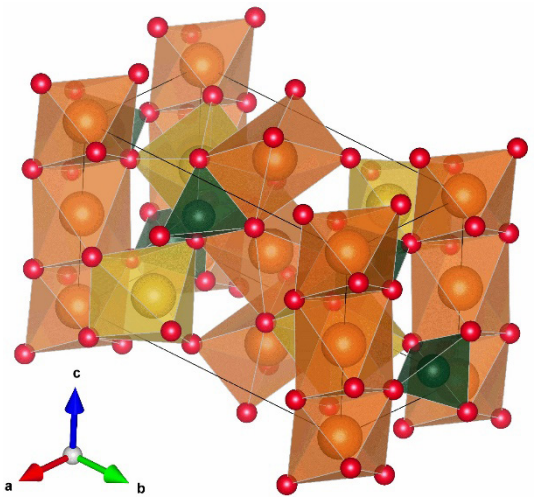

Fig. 2. Crystal structure of Mg_2SiO_4 material. Green tetrahedrons: $[SiO_4]$; orange and yellow octahedrons: $[MgO_6]$ [13].

Table 1. Ionic Radii of Mg^{2+}, Si^{4+}, Mn^{2+}, B^{3+}, Al^{3+}, Ga^{3+} and In^{3+} at Four-Fold and Six-Fold Coordination Given in Angstroms [20]

CN	Mg^{2+}	Si^{4+}	Mn^{2+}	B^{3+}	Al^{3+}	Ga^{3+}	In^{3+}
4	0.57		0.66	0.11	0.30	0.47	0.62
6		0.40	0.83	0.27	0.535	0.62	0.80

3.2. Persistent Luminescence Properties

If MGO samples are excited with X-rays, a broad luminescence band between 550–850 nm with two maximums at approximately 625 nm and 730 nm appears. When the excitation source is switched off, the afterglow with the same band characteristics continues for several hours. Figure 3a shows PersL spectra of MGO samples immediately after the cessation of irradiation. The luminescence signal is ascribed to the sum of two bands emerging from the Mn^{2+} optical transition from the excited state $^4T_1(^4G)$ to the ground state $^6A_1(^6S)$ when Mn^{2+} ions are in two non-equivalent Mg^{2+} positions in the host. Comparable results have been previously reported [12], [13].

Figure 3b shows the PersL decay curves of the MSO samples after irradiation with X-rays for 2 min depicted in a double-logarithmic plot. A strong afterglow signal can be detected for at least 6 h for all samples. It was concluded that, at least during measuring time, co-doping with B^{3+} did not improve the PersL properties of MSO: Mn^{2+} material. On the other hand, co-doping with Al^{3+}, Ga^{3+}, and In^{3+} increases the decay time of the PersL. Interestingly, a singly Mn^{2+} doped sample can be characterised by the highest initial intensity; however, out of all samples, it has the steepest decline in intensity, and after the first few minutes of removal of X-rays, PersL intensity of Al^{3+}, Ga^{3+}, and In^{3+} co-doped samples surpassed that of the MSO: Mn^{2+}.

PersL decay generally follows a power law: $I \sim t^{-n}$ which, in a double-logarithmic

scale, appears as a straight line with a slope of $-n$. It has been shown that if the n value is close to 1, the mechanism of PersL can be dominated by athermal tunnelling from the trapping site to a random distribution of recombination centres [21], [22]. A dashed line in Fig. 3b represents a slope of -1. All decay profiles fall close to that, especially in the later stages of the PersL decay ($t > 1\,h$); thus, it is reasonable to assume that tunnelling plays a significant role in the mechanism of PersL in MSO samples.

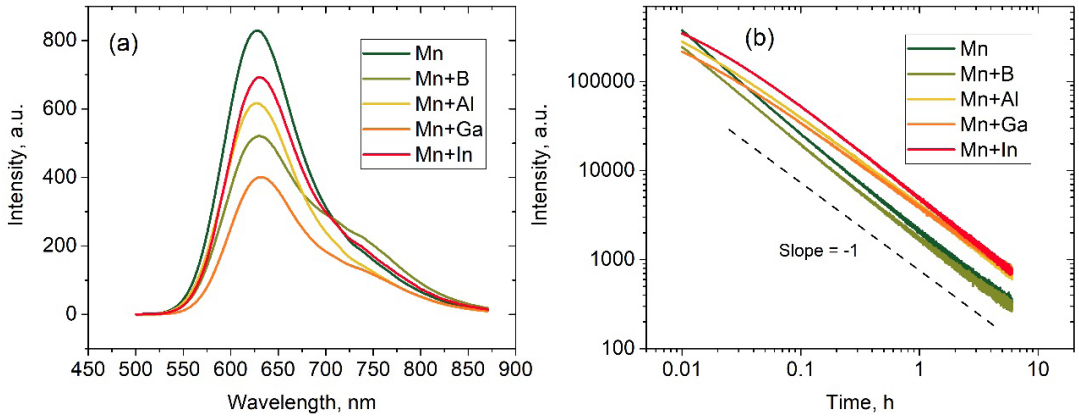

Fig. 3. (a) PersL spectra immediately after the cessation of excitation and (b) the afterglow decay curves of the MSO samples after irradiation with X-rays for 2 min, double-logarithmic plot.

3.3. Thermally Stimulated Luminescence and Trap Analysis

To analyse the trap properties of the MSO materials, thermally stimulated luminescence (TSL) glow curves after irradiation with X-rays were measured. The measurements were carried out by increasing temperature from room temperature up to 400 ºC with a heating rate of 1 ºC/s. The obtained TSL glow curves are presented in Fig. 4.

TSL is commonly acknowledged as one of the most efficient techniques for studying trap properties of PersL materials. The fundamental principles of the production of TSL are the same as those of PersL. Namely, some charge carriers are trapped by traps after irradiation but can be released via thermal detrapping if sufficient energy is accumulated. In the case of room temperature PersL, a signal with decaying intensity is observed. At the case of TSL, the material is typically heated with a constant heating rate. The emission signal usually increases and decreases throughout all measuring processes, with increases corresponding to the traps with a specific trap depth E_a, also called activation energy. In the end, a glow curve consisting of one or more glow peaks as $I = f(T)$ is obtained. A basic TSL glow curve may be used for the primary analysis of the trap properties. The position and intensity of each peak correspond to the trap depth and filled trap density, respectively. On the other hand, the number of glow peaks represents the number of different traps in the material [23].

In the case of the MSO samples, multiple glow peaks appear throughout all measured temperature region. For all samples, three principal glow peaks P1, P2, and P3 were noted with the only exception for Ga^{3+}

co-doped sample where P3 could not be ascribed to a specific peak since the TSL signal appears as a plateau throughout a broad temperature region; thus, P3 was divided into P3.1 (T_{max} = 240 ºC) and P3.2 (T_{max} = 340 ºC). For all samples, the most prominent peak is P2 with T_{max} around 130–180 ºC; precise values of T_{max} for all peaks are given in Table 2. This temperature range can be perceived as relatively high, and room temperature thermal detrapping probably is more dependent on P1 corresponding traps.

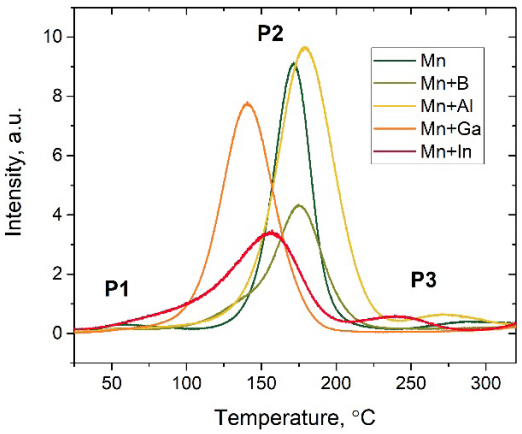

Fig. 4. TSL curves of MSO samples after irradiation with X-rays for 2 min. The heating rate applied: 1 °C/s.

For an in-depth trap analysis, a heating rate method, called Hoogenstraaten's method [24], [25], was applied. This technique evaluates the shift of the glow peak position depending on the heating rate. It is widely used to estimate the trap depth values. This method is based on analysing the set of TSL measurements for the same sample. For each measurement, the sample is irradiated with the same source for the same time, then TSL is measured using varied hating rates. Corresponding TSL glow curves of MSO samples are depicted in Fig. 5a–e, applied heating rates β = 0.25; 0.5; 1.0; 2.0; 4.0 *°C/s.* From each glow curve T_{max} – the temperature at the peak maximum intensity is noted. The relationship between heating rate β, glow peak position represented by T_{max} and trap depth E_a can be expressed by Eq. (1). Here, k_B is the Boltzmann constant and s is frequency factor – a temperature independent constant with a value in the order of the lattice vibration frequency, $10^{12} – 10^{14}$ s^{-1}.

$$\frac{\beta E_a}{k_B T_{max}^2} = s \cdot exp\left(\frac{E_a}{k_B T_{max}}\right). \quad (1)$$

From Eq. (1), if $ln\left(\frac{T_{max}^2}{\beta}\right)$ is plotted as a function of $\left(\frac{1}{k_B T_{max}}\right)$, a straight line with slope E_a should be obtained. Accordingly, the heating rate plots for all samples were obtained (Fig. 5f–j). Evaluated E_a values are given in Table 2. From here, several observations can be made. Firstly, there is a strong correlation between the initial intensity of PersL and the depth of the P1, an expected result since trap depths around 0.4–0.6 eV can be considered shallow and will effectively empty via thermal detrapping at the initial stages of PersL. On the other hand, P2 values fluctuate around 0.9 eV, this value can be perceived as somewhat deep, and effective thermal detrapping at room temperature would not be expected. P3 falls into the category of deep traps with an average trap depth around 1.1–1.6 eV and should not take part in the room temperature PersL process.

Figure 5k–o shows the results of the TSL fading experiment where TSL glow curves were measured after different delay time cessation of irradiation with the X-rays. For all MSO samples, shallow traps are emptied after the first hour, and the relative intensity of the P2 has also slightly decreased. At this point, the most likely origin of the PersL is athermal tunnelling, a conclusion is supported by PersL decay curves shown in Fig. 3b.

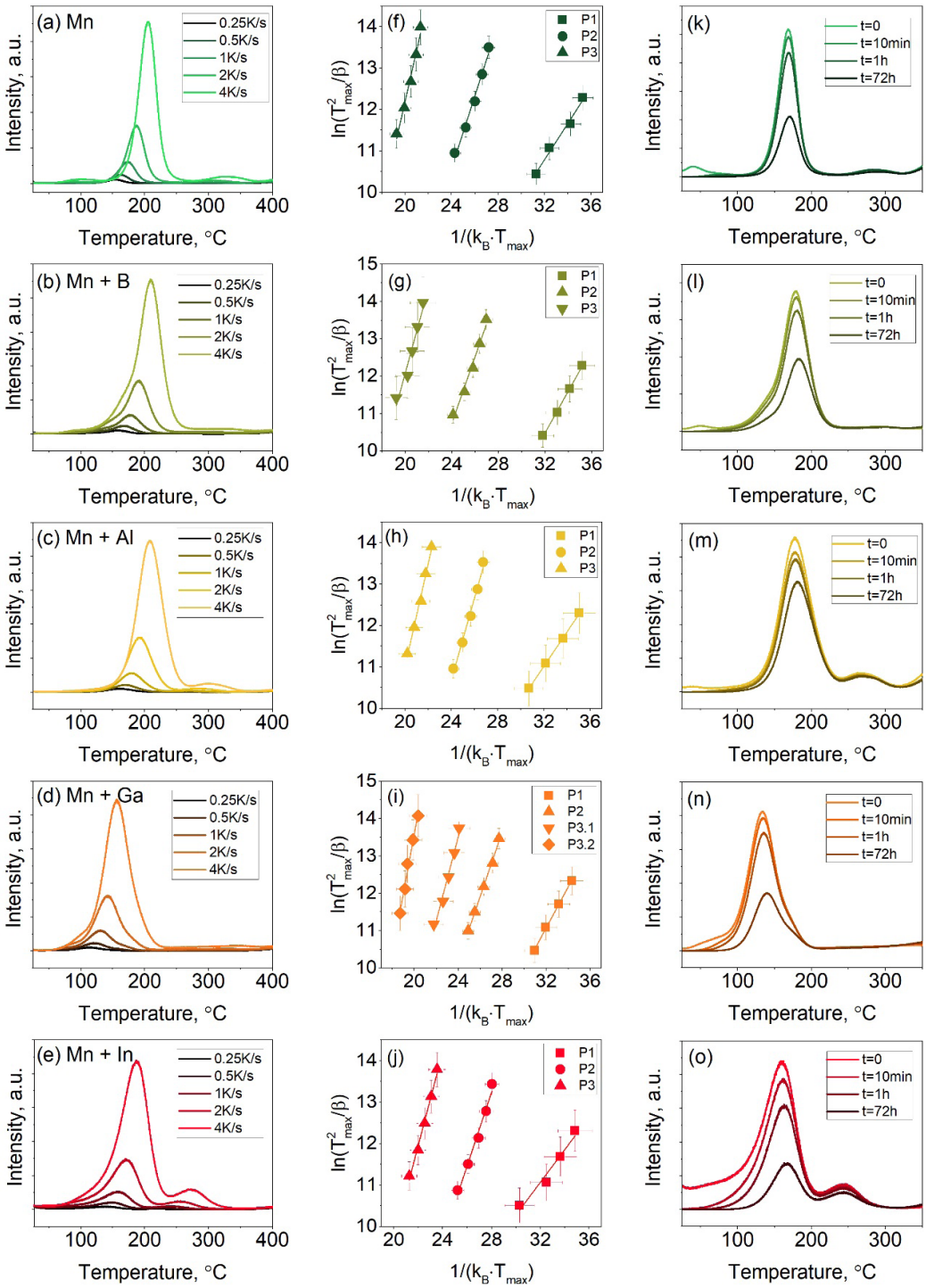

Fig. 5. TSL glow curves of MSO samples heated at different rates after irradiation with X-rays (a–e) and heating rate plots of the same samples (f–j). The glow peaks have been labelled as P1 to P3 from the lowest to the highest values. Fading of TSL glow curves of the same samples was measured after different delay times (k; l; m; n; o).

Table 2. Estimated Trap Depths E_a Derived from the Heating Rate Plots of the Corresponding TSL Peak and their T_{max} Value with Heating Rate 1 ºC/s.

Sample	Glow peak	T_{max}, °C	E_a, eV
MSO: Mn^{2+}	P1	40	0.44 ± 0.04
	P2	170	0.87 ± 0.06
	P3	284	1.24 ± 0.09
MSO: Mn^{2+}; B^{3+}	P1	48	0.56 ± 0.02
	P2	178	0.89 ± 0.07
	P3	290	1.14 ± 0.14
MSO: Mn^{2+}; Al^{3+}	P1	41	0.41 ± 0.03
	P2	178	0.99 ± 0.06
	P3	269	1.24 ± 0.06
MSO: Mn^{2+}; Ga^{3+}	P1	60	0.55 ± 0.01
	P2	133	0.92 ± 0.09
	P3.1	240	1.12 ± 0.09
	P3.2	340	1.60 ± 0.12
MSO: Mn^{2+}; In^{3+}	P1	55	0.39 ± 0.06
	P2	160	0.89 ± 0.07
	P3	243	1.13 ± 0.06

4. CONCLUSIONS

In conclusion, Mg_2SiO_4 material doped with 0.1 mol% Mn^{2+} and co-doped with 0.5 mol% B^{3+} or Al^{3+} or Ga^{3+} or In^{3+} was successfully synthesized by a solid-state reaction method.

A strong red Mn^{2+} luminescence and afterglow with two maximums at around 625 nm and 730 nm can be observed when excited with X-rays for at least six hours. Furthermore, adding Al^{3+}, Ga^{3+}, or In^{3+} improves PersL intensity at later stages of the PersL process.

TSL analysis revealed that there were at least three different charge carrier traps in each sample with average activation energies varying from 0.4 eV to 1.2 eV, and the first two of these traps played a role in the room temperature PersL mechanism, which likely included not only thermal detrapping but also athermal tunnelling of charge carriers.

ACKNOWLEDGEMENTS

The Institute of Solid State Physics, University of Latvia, as the Center of Excellence has received funding from the European Union's Horizon 2020 Framework Programme H2020-WIDESPREAD-01-2016-2017-TeamingPhase2 under grant agreement No. 739508, project CAMART².

REFERENCES

1. Vitola, V., Millers, D., Bite, I., Smits, K., & Spustaka, A. (2019). Recent Progress in Understanding the Persistent Luminescence in $SrAl_2O_4$: Eu,Dy. *Materials Science and Technology (United Kingdom)*, *35* (14), 1661–1677. DOI:10.1080/02670836.2019.1649802
2. Richard, C., & Viana, B. (2022). Persistent X-Ray-Activated Phosphors: Mechanisms and Applications. *Light: Science & Applications*, *11* (1), 123. DOI:10.1038/s41377-022-00808-6
3. Jain, A., Kumar, A., Dhoble, S. J., & Peshwe, D. R. (2016). Persistent Luminescence: An Insight. *Renewable and Sustainable Energy Reviews*, *65*, 135–153. DOI:10.1016/j.rser.2016.06.081
4. Li, Y., Gecevicius, M., & Qiu, J. (2016). Long Persistent Phosphors – From Fundamentals to Applications. *Chemical Society Reviews*, *45* (8), 2090–2136. DOI:10.1039/C5CS00582E
5. Poelman, D., Van der Heggen, D., Du, J., Cosaert, E., & Smet, P. F. (2020). Persistent Phosphors for the Future: Fit for the Right Application. *Journal of Applied Physics*, 128 (24), 240903. DOI:10.1063/5.0032972
6. Liang, Y., Liu, F., Chen, Y., Wang, X., Sun, K., & Pan, Z. (2017). Extending the Applications for Lanthanide Ions: Efficient Emitters in Short-Wave Infrared Persistent Luminescence. *Journal of Materials Chemistry C*, *5* (26), 6488–6492. DOI:10.1039/C7TC01436H
7. Wang, X., Zhang, Z., Tang, Z., & Lin, Y. (2003). Characterization and Properties of a Red and Orange Y2O2S-Based Long Afterglow Phosphor. *Materials Chemistry and Physics*, *80* (1), 1–5. DOI:10.1016/S0254-0584(02)00097-4
8. Gartia, R. K., & Chandrasekhar, N. (2016). Physical Basis of Persistent Luminescence: The Case of Europium Doped $Ca_{1-x}Sr_xS$. *Journal of Alloys and Compounds*, *683*, 157–163. DOI:10.1016/j.jallcom.2016.05.087
9. Zhuang, Y., Ueda, J., & Tanabe, S. (2014). Multi-Color Persistent Luminescence in Transparent Glass Ceramics Containing Spinel Nano-Crystals with Mn^{2+} Ions. *Applied Physics Letters*, *105* (19), 3–7. DOI:10.1063/1.4901749
10. Kong, J., Zheng, W., Liu, Y., Li, R., Ma, E., Zhu, H., & Chen, X. (2015). Persistent Luminescence from Eu^{3+} in SnO_2 Nanoparticles. *Nanoscale*, *7* (25), 11048–11054. DOI:10.1039/c5nr01961c
11. Pihlgren, L., Laihinen, T., Rodrigues, L. C. V., Carlson, S., Eskola, K. O., Kotlov, A. ... & Hölsä, J. (2014). On the Mechanism of Persistent Up-conversion Luminescence in the ZrO_2: Yb^{3+},Er^{3+} Nanomaterials. *Optical Materials*, *36* (10), 1698–1704. DOI:10.1016/j.optmat.2014.01.027
12. Lin, L., Yin, M., Shi, C., & Zhang, W. (2008). Luminescence Properties of a New Red Long-lasting Phosphor: Mg_2SiO_4: Dy^{3+}, Mn^{2+}. *Journal of Alloys and Compounds*, *455* (1–2), 327–330. DOI:10.1016/j.jallcom.2007.01.059
13. Doke, G., Krieke, G., Antuzevics, A., Sarakovskis, A., & Berzina, B. (2023). Optical Properties of Red-Emitting Long Afterglow Phosphor $Mg_2Si_{1-x}Ge_xO_4$: Mn^{2+}/Mn^{4+}. *Optical Materials*, *137*, 113500. DOI:10.1016/j.optmat.2023.113500
14. Jia, D., & Yen, W. M. (2003). Enhanced V_K^{3+} Center Afterglow in $MgAl_2O_4$ by Doping with Ce^{3+}. *Journal of Luminescence*, *101* (1–2), 115–121. DOI:10.1016/S0022-2313(02)00394-0
15. Vitola, V., Lahti, V., Bite, I., Spustaka, A., Millers, D., Lastusaari, M., ... & Smits, K. (2021). Low Temperature Afterglow from $SrAl_2O_4$: Eu, Dy, B Containing Glass. *Scripta Materialia*, *190*, 86–90. DOI:10.1016/j.scriptamat.2020.08.023
16. Zhou, D., Song, Z., Zhou, H., & Liu, Q. (2020). Enhanced Persistent Luminescence via Si^{4+} Co-doping in $Y_3Al_2Ga_3O_{12}$: Ce^{3+}, Yb^{3+}, B^{3+}. *Journal of Luminescence*, *222*, 117190. DOI:10.1016/j.jlumin.2020.117190

17. Noto, L. L., Pitale, S. S., Gusowki, M. A., Terblans, J. J., Ntwaeaborwa, O. M., & Swart, H. C. (2013). Afterglow Enhancement with In3+ Codoping in $CaTiO_3$: Pr^{3+} Red Phosphor. *Powder Technology*, *237* (3), 141–146. DOI:10.1016/j.powtec.2013.01.029

18. Doke, G., Kalnina, A., Cipa, J., Springis, M., & Sarakovskis, A. (2022). Optical Properties of Near Infrared Persistent Phosphor $CaZnGe_2O_6$: Cr^{3+}, M^{3+} (M^{3+} = B^{3+}; Al^{3+}; Ga^{3+}). *Solid State Communications*, *354*, 114894. DOI:10.1016/j.ssc.2022.114894

19. Awad, A., Koster Van Groos, A. F., & Guggenheim, S. (2000). Forsteritic Olivine: Effect of Crystallographic Direction on Dissolution Kinetics. *Geochimica et Cosmochimica Acta*, *64* (10), 1765–1772. DOI:10.1016/S0016-7037(99)00442-1

20. Shannon, R. D. (1976). Revised Effective Ionic Radii and Systematic Studies of Interatomic Distances in Halides and Chalcogenides. *Acta Crystallographica Section A*, *32* (5), 751–767. DOI:10.1107/S0567739476001551

21. Avouris, P., & Morgan, T. N. (1981). A Tunneling Model for the Decay of Luminescence in Inorganic Phosphors: The Case of Zn_2SiO_4: Mn. *The Journal of Chemical Physics*, *74* (8), 4347–4355. DOI:10.1063/1.441677

22. Doke, G., Antuzevics, A., Krieke, G., Kalnina, A., & Sarakovskis, A. (2022). Novel Broadband Near-Infrared Emitting Long Afterglow Phosphor $MgGeO_3$: Cr^{3+}. *Journal of Alloys and Compounds*, *918*, 165768. DOI:10.1016/j.jallcom.2022.165768

23. Bos, A. J. J. (2006). Theory of Thermoluminescence, *Radiation Measurements*, *41*, S45–S56. DOI:10.1016/j.radmeas.2007.01.003

24. Rasheedy, M. S. (2005). Method of Hoogenstraaten as a Tool for Obtaining the Trap Parameters of General-Order ThermoluminescenceGlowPeaks.*Radiation Effects and Defects in Solids*, *160* (9), 383–390. DOI:10.1080/10420150500459999

25. Doke, G., Antuzevics, A., Krieke, G., Kalnina, A., Springis, M., & Sarakovskis, A. (2021). UV and X-Ray Excited Red Persistent Luminescence in Mn^{2+} Doped $MgGeO_3$ Material Synthesized in Air and Reducing Atmosphere. *Journal of Luminescence*, *234*, 117995. DOI:10.1016/j.jlumin.2021.117995